communications biology

A Nature Portfolio journal

Article

https://doi.org/10.1038/s42003-025-07748-y

Genomic diversity of *mcr*-carrying plasmids and the role of type IV secretion systems in IncI2 plasmids conjugation

Zhe Li[1], Zhenpeng Li[1], Yao Peng[1], Mengke Zhang[1,2], Yuanxi Wen[1,3], Xin Lu[1,4] ✉ & Biao Kan[1,4] ✉

The rapid dissemination of colistin resistance via *mcr*-carrying plasmids (pMCRs) poses a significant public health challenge. This study examined the genomic diversity and conjugation mechanisms of pMCRs, with a particular focus on the role of type IV secretion systems (T4SS) in IncI2 plasmids. The 868 complete plasmid sequences revealed various replicon types of pMCRs, with IncI2 as the primary epidemic type, and the co-transfer risk of multidrug resistance genes associated with IncHI2. T4SS was identified in 89.9% of pMCRs, with the T4SS sequence exclusively carried by IncI2 being conserved and typical of the VirB/D4 type, consisting of 12 subunits. Conjugation assays confirmed the essential role of the pilus subunit VirB2 and the significant impact of $VirB5_{P3}$ on conjugation. This was further validated in the in vivo intra-species competitive conjugation of *Escherichia coli*. Structural predictions show that a hypervariable region at the C-terminus of the pentameric VirB5 co-evolves in sequence with VirB6, and the conserved N-terminal may act as a potential drug target to inhibit the plasmid transfer channel. This study will deepen the understanding of the pMCR epidemic patterns and provide additional insights for controlling the spread of resistant plasmids.

The rising antibiotic resistance of multidrug-resistant (MDR) Gram-negative bacteria poses a significant threat to public health[1]. In response to delays in developing new antimicrobials, colistin has been reintroduced as a 'last-resort' antibiotic for MDR Enterobacteriaceae infections, despite its toxicity and poor renal clearance[2]. By late 2015, the plasmid-borne *mcr-1* gene (pMCR-1) was identified as a driver of colistin resistance[3], undermining the efficacy of colistin-related antibiotics and complicating treatment. The *mcr-1* gene encodes phosphoethanolamine transferase, reducing the affinity between lipid A and polymyxins by adding phosphoethanolamine to lipid A. These colistin-resistant plasmids spread rapidly and may incur lower fitness costs[4,5], unlike earlier resistance tied to chromosomal gene mutations and regulatory changes[6,7].

The plasmid-driven spread of colistin resistance underscores the global challenge of antibiotic resistance[8], with ten *mcr* variants identified in over 50 countries[9–11], often co-transferred with other resistance genes like carbapenemases[12,13] and extended-spectrum β-lactamases[14,15]. The ban on colistin as a feed additive in many regions has reduced *mcr-1* prevalence[16], indicating that its extensive use in animals has been a key driver. However, *mcr* persists at low levels, likely due to co-selection by other antimicrobials[17]. In clinical settings, rising carbapenem resistance and limited treatment options have led to a greater reliance on colistin as a last-line therapy. Therefore, it is necessary to elucidate the epidemic patterns of *mcr* and sustain surveillance of polymyxin resistance spread.

The *mcr* genes are carried by various plasmids, with over 20 types of *mcr-1* carrying plasmids reported, involving replicon types such as IncI2, IncX4, and IncHI2. IncI2 plasmids are considered the optimal vectors for *mcr-1* dissemination[18] and represent the first reported replicon type of *mcr-1* plasmids. Conjugative *mcr* plasmids pose a greater threat due to their spontaneous cross-host transfer capability. The conjugation process is generally considered to be mediated by a type IV secretion system (T4SS) encoded by plasmids or chromosomes, where DNA or virulence proteins[19–21] are transferred into recipient cells through specialized pilus assembled by this macromolecular assemblies[22]. This secretion system superfamily exhibits genetic and functional heterogeneity, complicating classification[22]. One scheme categorizes systems into F-type (Type IVA), P-type (Type IVA), or I-type (Type IVB)based on pilus type[19]. F- and P-type systems share a conserved set of ~12 subunits homologous to the *Agrobacterium tumefaciens* VirB/VirD4 system[23]; I-type systems, represented by the *Legionella pneumophila* Dot/Icm system, involve over 25 proteins with limited similarity to VirB components[24]. The VirB/VirD4 components are

[1]National Key Laboratory of Intelligent Tracking and Forecasting for Infectious Diseases, National Institute for Communicable Disease Control and Prevention, Chinese Center for Disease Control and Prevention, Beijing, China. [2]School of Light Industry Science and Engineering, Beijing Technology and Business University, Beijing, China. [3]School of Public Health, Cheeloo College of Medicine, Shandong University, Jinan, Shandong, China. [4]These authors jointly supervised this work: Xin Lu, Biao Kan. ✉e-mail: luxin@icdc.cn; kanbiao@icdc.cn

considered 'minimized'[25] and most representative T4SS. VirB7, VirB9, and the C-terminus of VirB10 form the outer-membrane complex (OMCC)[26,27], which connects to the inner-membrane complex (IMC) comprising VirB3, VirB6, VirB8, and the N-terminus of VirB10[28]. Three ATPases (VirD4, VirB4, and VirB11) power the system and can interact directly with the IMC[29]. The pilus subunit VirB2 is extracted from the inner membrane to the VirB6 platform at the periplasmic assembly site, where repeated recruitment and integration progressively elongate the pilus, simultaneously driving VirB5 upward until it traverses the outer membrane into the extracellular environment[30]. VirB5 is retained at the tip of the pilus, where it binds to specific receptors on the surface of the target cell or directly embeds into the target cell membrane. The functional homolog of VirB5 in the Cag system, CagL, has been shown to bind integrins on the surface of human cells[31]. The Conjugative pilus serves as channels for the horizontal transfer of antibiotic-resistant plasmids such as pMCR, and their biological function is a key component in the study of the molecular mechanisms underlying plasmid horizontal transfer.

This study utilized plasmid complete genomes from the existing NCBI database and those assembled in our laboratory to systematically reveal the genomic and epidemiological characteristics of the all-variant pMCRs. Risk warnings are proposed regarding high-risk host carriers, major epidemic plasmid types, co-transfer of resistant genes, plasmid plasticity, plasmid fusion, and spontaneous transfer. On the other hand, through the diversity and functional analysis of the T4SS gene clusters carried by pMCRs, the indispensable contribution of T4SS to the spread of pMCRs and the oligomerization of the conjugative pilus subunits, as well as the preference for recipient bacteria transfer, have been demonstrated. This provides evidence for the preferential transfer of IncI2 pMCR.

Results

pMCRs have a host preference for Enterobacteriaceae and a high carrying rate of T4SS

The genomes of 868 pMCR were associated with 733 biosample entries, with 569 having recorded isolation sources. The sources are mainly human (335/733, 45.7%), covering various domains related to human survival, indicating the formation of a complete network of colistin resistance transmission between the environment, animals, food, and humans (Supplementary Fig. 1). Among these, a description of a pMCR carried by *Enterobacter hormaechei* isolated from a post-disinfection environmental swab in the hospital ICU alerts to the burden of antibiotic-resistant plasmids in nosocomial infections and the necessity of implementing post-disinfection microbial monitoring and cultivation[32].

Inc types in pMCRs: More than 63 Inc types were identified in 868 pMCRs (Fig. 1, Supplementary Data 1). The three major types were IncI2 (28.1%), IncHI2 (25.5%), and IncX4 (18.4%) (Fig. 2). Plasmid fusion was present in 93 (10.7%) plasmids and 38 types (60.3%). Fusions of two (22/38) or three (12/38) Inc types were common, and up to five Inc types were identified in one plasmid (1/38) (Fig. 3). The length of pMCRs ranged from 5.3 to 477.3 kb, and fusion plasmids were usually longer than single plasmids (Fig. 3). IncHI2, IncFII(K), and IncFIB(K) plasmids span a wide range of lengths and are major contributors to fusion plasmids, indicating the active genomic integration capability of these plasmids (Fig. 3). In contrast, IncI2, IncX4, and IncP1 plasmids are smaller and more fixed in size, generally ranging from 30 to 60 kbp (Fig. 3), although fusion of IncI2 and IncX4 has also been observed (MT929289.1). Plasmid pan-genome curves were created for the Inc types containing more than 30 plasmids (IncI2, IncHI2, IncX4, and IncP1) (Fig. 4). Power law exponents were estimated by least-squares linear regression, and the distributions fit the equation $y = kx^{\gamma}$, where γ was 0.235, 0.293, 0.317, and 0.259, respectively (Fig. 4), indicating open pan-genomes according to Heaps' law[33,34]. This suggests that the four major plasmid types of pMCR exhibit genomic diversity and continue to integrate new genetic elements.

Co-occurrence of antimicrobial resistance genes (ARGs) in pMCRs: ARGs carried by the four major Inc-type plasmids (IncI2, IncHI2, IncX4, and IncP1) in the dataset were identified to evaluate the risk of multidrug resistance of each Inc-type pMCR and the co-occurrence of ARGs with *mcr* genes (Supplementary Fig. 2). IncHI2 carries a significantly higher number and diversity of ARGs compared to the other three types (Fig. 4 and Supplementary Fig. 2). This characteristic aligns with the statistical analysis of plasmid length (Figs. 3 and 4, and Supplementary Fig. 2). A total of 15 classes of antibiotic resistance genes were identified, including Aldehyde, Aminocyelitol, Aminoglycoside, Amphenicol, Beta-lactam, Chloramphenicol-florfenicol, Folate pathway antagonist, Fosfomycin, Lincosamide, Macrolide, Polymyxin, Quaternary ammonium compound, Quinolone, Rifamyein, and Tetracycline (Supplementary Fig. 2). Except for chloramphenicol-florfenicol, the other 14 classes were identified in IncHI2 pMCR (Supplementary Fig. 2). Co-carrying of *mcr* and β-lactamase genes were observed in all four plasmid types, suggesting a reduced efficacy of polymyxins in treating β-lactam-resistant bacteria. Additionally, eight classes of antibiotic resistance genes, including beta-lactam, tetracycline, and

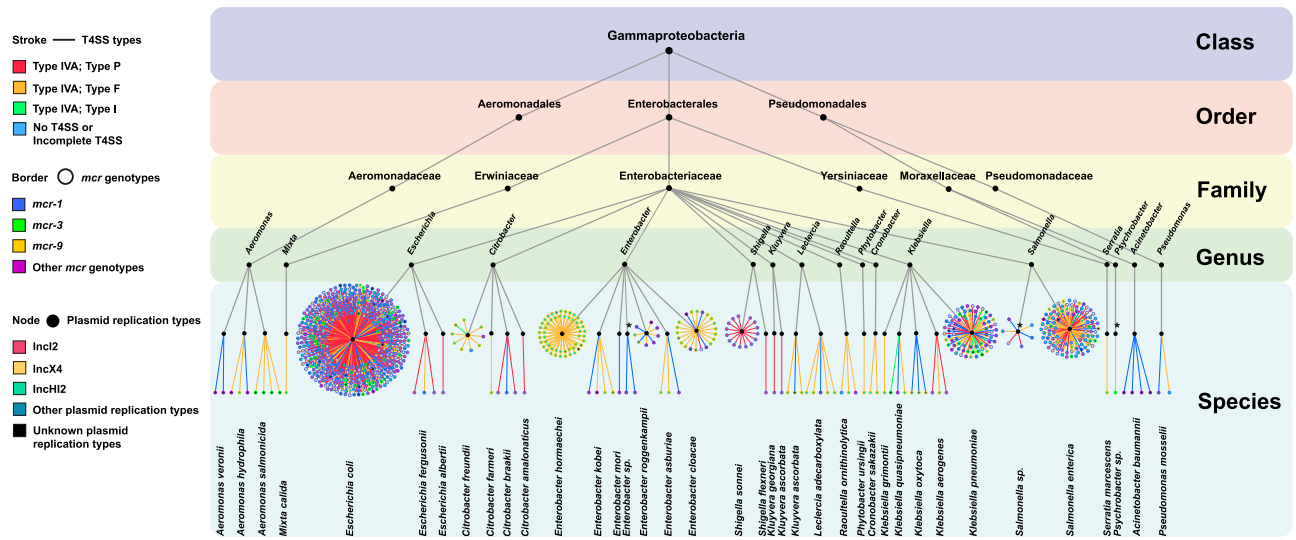

Fig. 1 | Genomic characteristics (plasmid replication types, *mcr* genotypes, and T4SS types) and host distribution of *mcr*-carrying plasmids. The data are based on the complete genomes of 868 pMCRs and their corresponding sample isolation information. The plasmid hosts are arranged from the Class level to the Species level. The species-level region (in blue) represents each pMCR by a point-line combination: "Stroke" represents T4SS types, "Border" represents *mcr* genotypes, and "Node" represents plasmid replicon types. Asterisk (*) represents strains with *Species indeterminata*. The network was drawn using Cytoscape version 3.6.0.

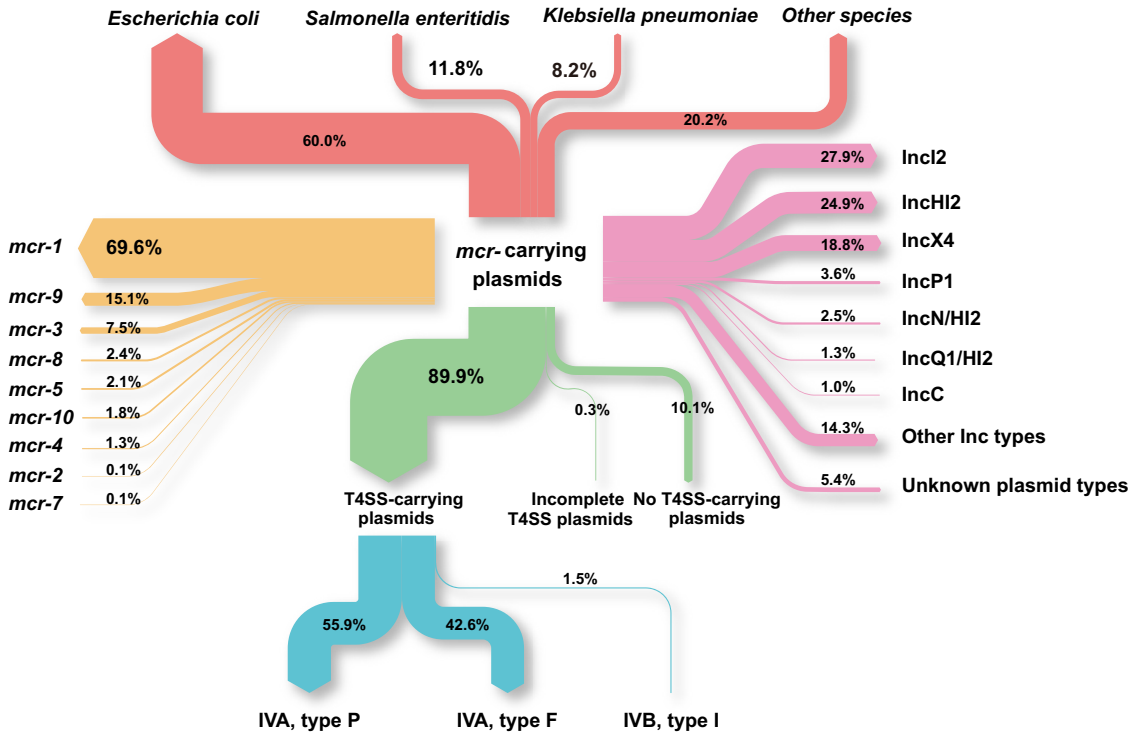

Fig. 2 | Sankey diagram of bacterial hosts, *mcr* genotypes, plasmid replication types, and T4SS types in 868 completed genomes of *mcr*-carrying plasmids. The proportions of each type are labeled within the arrows. "Unknown plasmid types" means: no known plasmid replicon type was identified. The figure was drawn using e!Sankey 5.

polymyxin, were identified in an IncHI2 plasmid (GenBank accession number: CP025402.1) isolated from human respiratory secretions. The co-carrying of *tet(X)* and *mcr-1.1* indicates the possible ineffectiveness of two last-resort drugs (tigecycline and polymyxin) used to treat carbapenem-resistant bacteria in clinical settings. The four major replicon types of pMCR all carry the risk of co-transfer of resistance genes, with IncHI2 carrying the highest number and variety of resistance genes.

Bacterial hosts of pMCRs: All the bacterial hosts of pMCRs in the dataset belonged to *Gammaproteobacteria*, with 17 genera and 34 species (Fig. 1). Approximately 98% of plasmids were found in the Enterobacteriaceae family. The predominant species were *E. coli* (60%), *S. enteritidis* (11.8%), and *K. pneumoniae* (8.2%) (Fig. 2), indicating a preferential transfer of pMCR to Enterobacteriaceae hosts. The pMCR carried by these three host species shows diversity in *mcr* subtypes, plasmid types, and Inc types. (Fig. 1 and Supplementary Fig. 3). Conversely, some species carry more conserved pMCR, exhibiting consistency in the aforementioned features, such as *Enterobacter hormaechei* and *Shigella sonnei* (Fig. 1). These findings highlight the differences in the storage and carriage of pMCR in various host species, with Enterobacteriaceae, especially *E. coli*, being the most suitable.

mcr genotypes of pMCRs: Currently, nine *mcr-1* homologs (*mcr-2* to *mcr-10*) have been identified. Phylogenetic analysis shows that MCR-1 has high amino acid sequence similarity with MCR-2 (81%) and MCR-6 (83%), placing them in the same subgroup. However, based on their amino acid homology, MCR-3 (32%), MCR-4 (34%), MCR-7 (35%), MCR-8 (31%), MCR-9 (36%), and MCR-10 (36%) form a separate subgroup. Compared to other members, MCR-5 (36%) forms a distinct subgroup due to its lower amino acid homology[16]. Nine *mcr* genotypes (except *mcr-6*) were found in 868 pMCRs, and the most prevalent genes were *mcr-1* (approximately 69.6%), *mcr-9* (15.1%), and *mcr-3* (7.5%) (Fig. 2). In addition, 28 of 63 Inc plasmids carried the *mcr-1* gene. *mcr-1* is predominantly found in *Escherichia*, *Salmonella*, *Klebsiella*, and *Shigella*, whereas *mcr-3* and *mcr-9* are associated with *Aeromonas*, *Enterobacter*, *Acinetobacter*, and *Leclercia*. (Figs. 1 and 5). Thus, *mcr-1* is the dominant circulating genotype, and its transmission preference may have played a key role in enterobacteria, particularly within the family Enterobacteriaceae, becoming the main carriers of pMCR[16].

T4SS gene clusters in pMCRs: In the dataset, T4SS gene clusters were found in 89.9% plasmids, with a predominance of types P (434, 55.9%) and F (331, 42.6%) (Fig. 2). I-type was found in *K. pneumoniae* and *E. coli* and accounted for 1.5% of T4SS sequences. There was a clear association between T4SS subtypes and three Inc types (IncI2, IncHI2, and IncX4, Fig. 5). IncI2 and IncX4 exclusively carried P-type T4SS ($T4SS_P$), while IncHI2 exclusively carried F-type T4SS ($T4SS_F$). The strong correlation between Inc types and T4SS subtypes suggests that the T4SS gene cluster is an inherent component of each plasmid type, rather than being acquired.

Plasmids carrying different T4SS subtypes had distinctive host distributions. For instance, $T4SS_P$-carrying pMCRs were found in 14 bacterial species, with 31.0 plasmids per species and a predominance in *E. coli* (80%) (Fig. 5). In contrast, $T4SS_F$-carrying pMCRs were found in 28 species, with 11.8 plasmids per species, which corresponded a wider host range (Fig. 5).

The proportion of plasmids carrying each *mcr* genotype reflected to some extent the prevalence of the genotypes. We observed a positive correlation between the T4SS carriage rate and the proportion of *mcr* genotypes (Supplementary Fig. 4, Pearson correlation 0.9998). Significantly, the T4SS gene cluster carriage rates of the two dominant genotypes, *mcr-1* and *mcr-9*, are around 95%, while no T4SS gene cluster was identified on plasmids carrying *mcr-4* (Supplementary Fig. 4). Among them, the $T4SS_P$ is mainly carried by pMCR-1 (95.9%) and pMCR-3 (3.5%), while 93.9% of pMCR-9 carries the $T4SS_F$ (Supplementary Fig. 4). For plasmids of other *mcr* genotypes, no clear correspondence was observed due to limited quantities. The carrying rate of T4SS is positively correlated with the proportion of *mcr* genotypes, suggesting that the presence of T4SS may contribute to the spread advantage of *mcr-1*, *mcr-9*, and *mcr-3*.

$T4SS_{P3}$ had highly conserved core gene homology and gene cluster organization

A total of 434 pMCRs had $T4SS_P$, and the coding genes presented three composition modes: the *trb* gene cluster, the shorter *virB/virD4* gene cluster

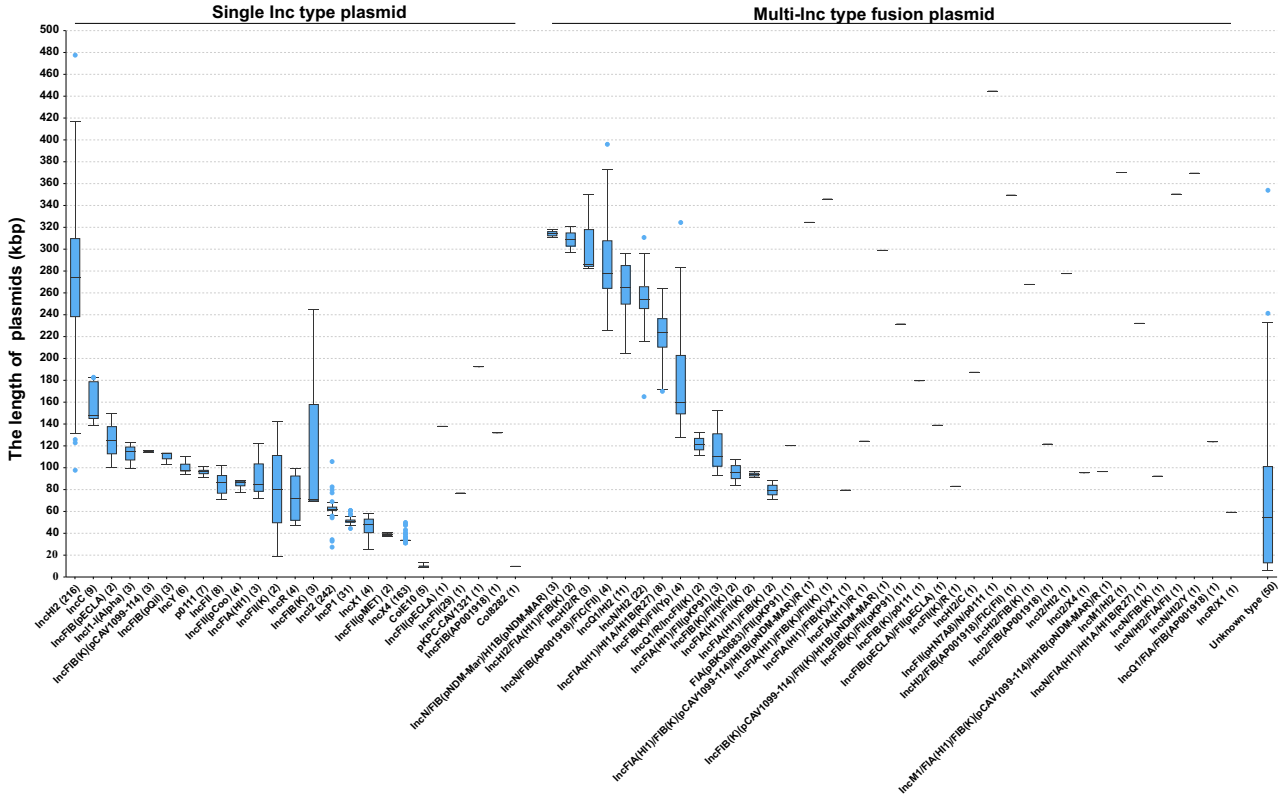

Fig. 3 | Length of *mcr*-carrying plasmids belonging to different plasmid replication types. The lengths of plasmids with different replicon types are represented using box plots. The line inside the box represents the median. The "whiskers" outside the box typically extend to 1.5 times the interquartile range beyond the box, representing data dispersion. Types with a sample size of one are represented by a short line. Dots represent outliers. The sample count is indicated in parentheses after the plasmid types. The data is provided in the Supplementary Data 1 (https://doi.org/10.5281/zenodo.14861845).

and the typical *virB/virD4* gene cluster contained 11, 10, and 12 core genes, respectively. Using amino acid sequences of these 33 genes as references for cluster analysis, the plasmids were divided into three groups with specific gene compositions: $T4SS_{P1}$, $T4SS_{P2}$, and $T4SS_{P3}$ (Fig. 6). Gene sequences were conserved within each group. Only fusion plasmids carried more than one type of T4SS gene cluster. Although $T4SS_{P2}$ and $T4SS_{P3}$ were annotated as the *virB/virD4* gene cluster, low sequence homology, and different gene compositions suggest that these clusters may be inherent components of the plasmids rather than acquired ones.

We analyzed the diversity of gene arrangements in $T4SS_{P3}$. A total of 240 plasmids were divided into 37 subtypes, from subtype 1 (72.2%) to subtype 37 (0.4%) (Fig. 7a). Similar to $T4SS_{A.tumefaciens}$, $T4SS_{R388}$, and $T4SS_{KM101}$, $T4SS_{P3}$ had 12 core genes (Fig. 7b); however, *virB5* and *virB6* were independent of the other 10 genes and were located 4 kb upstream of *virB1* (Fig. 7b). In addition, considering the inverse arrangement of *virB5* and *virB6* (Fig. 7b), $T4SS_{P3}$ may contain genetic elements from different sources.

Inc types were highly conserved in $T4SS_{P3}$ (Fig. 7c). Although $T4SS_{P3}$ had multiple subtypes, gene arrangement patterns, Inc types, and gene clusters were highly conserved (Fig. 7c). $T4SS_F$ and $T4SS_{P3}$ were detected in the IncI2 and IncHI2 fusion plasmid MH522426.1. (Fig. 7a, subtype 37). The plasmids were distributed across 13 species, with a predominance in *E. coli* (80.9%). Moreover, there was no significant correlation between T4SS subtypes and bacterial hoses (Fig. 7c). Although $T4SS_{P3}$ includes several subtypes, the gene cluster composition is generally consistent, with high homology among the subunits (Fig. 7c).

The sequence diversity of the $T4SS_{P3}$ gene cluster is mainly reflected in $VirB5_{P3}$ (VirB5 in $T4SS_{P3}$) and $VirB6_{P3}$ (VirB6 in $T4SS_{P3}$) (Supplementary Fig. 5). A corresponding relationship was shown between the sequence types of the two proteins, which was similar to co-evolution (Supplementary Fig. 5). In plasmids carrying the complete T4SS gene cluster, Pearson correlation coefficients (PCCs) between elements were calculated based on the identity with the reference sequences. The PCC of sequence types between $VirB5_{P3}$ and $VirB6_{P3}$ was 0.96, indicating a strong correlation (Supplementary Fig. 6).

The self-transfer of pMCRs carrying $T4SS_{P3}$ depends on $VirB2_{P3}$ and $VirB5_{P3}$

The high carrying rate of T4SS suggests that pMCRs can generally transfer themselves depending on conjugation. Therefore, the role of pMCR-encoded T4SS in plasmid self-transfer was estimated using conjugation assays. Two IncI2 plasmids, pSH13G841 and pSH12G402, isolated from *S.* Typhimurium, were used as the transfer plasmids in this experiment. They were isolated from *S.* Typhimurium strains collected during a surveillance study conducted at a diarrheal clinic in Shanghai, China[35]. The samples were fecal samples from children under one year of age. They encode $T4SS_{P3}$ (subtype 1) and contain resistance genes *mcr-1.1* (Supplementary Fig. 7). In conjugation experiments, *E. coli* J53 harboring pSH13G841 and pSH12G402, respectively, served as donor strains in two parallel experiments, forming conjugation pairs with three Enterobacteriaceae species (three strains each of *E. coli*, S. Typhimurium, and *K. pneumoniae*). The growth rate of each recipient strain was similar (Supplementary Fig. 8). The conjugative plasmids can be transferred to all recipient bacteria; however, transfer efficiency varied across species, ranging from 10^{-2} to 10^{-3} between *E. coli* and *K. pneumoniae* (*E. coli* vs *K. pneumoniae* $p > 0.9999$, $n = 9$) and around 10^{-5} in *S.* Typhimurium (*S.* Typhimurium vs *E. coli* or *K. pneumoniae* $p < 0.0001$, $n = 9$) (Fig. 8). In contrast, the T4SS absent plasmid p841DEL*T4SS* (or p402DEL*T4SS*) was not transferred in the analyzed conjugation pairs, suggesting that pMCR-encoded T4SS was essential for conjugative transfer (Fig. 8).

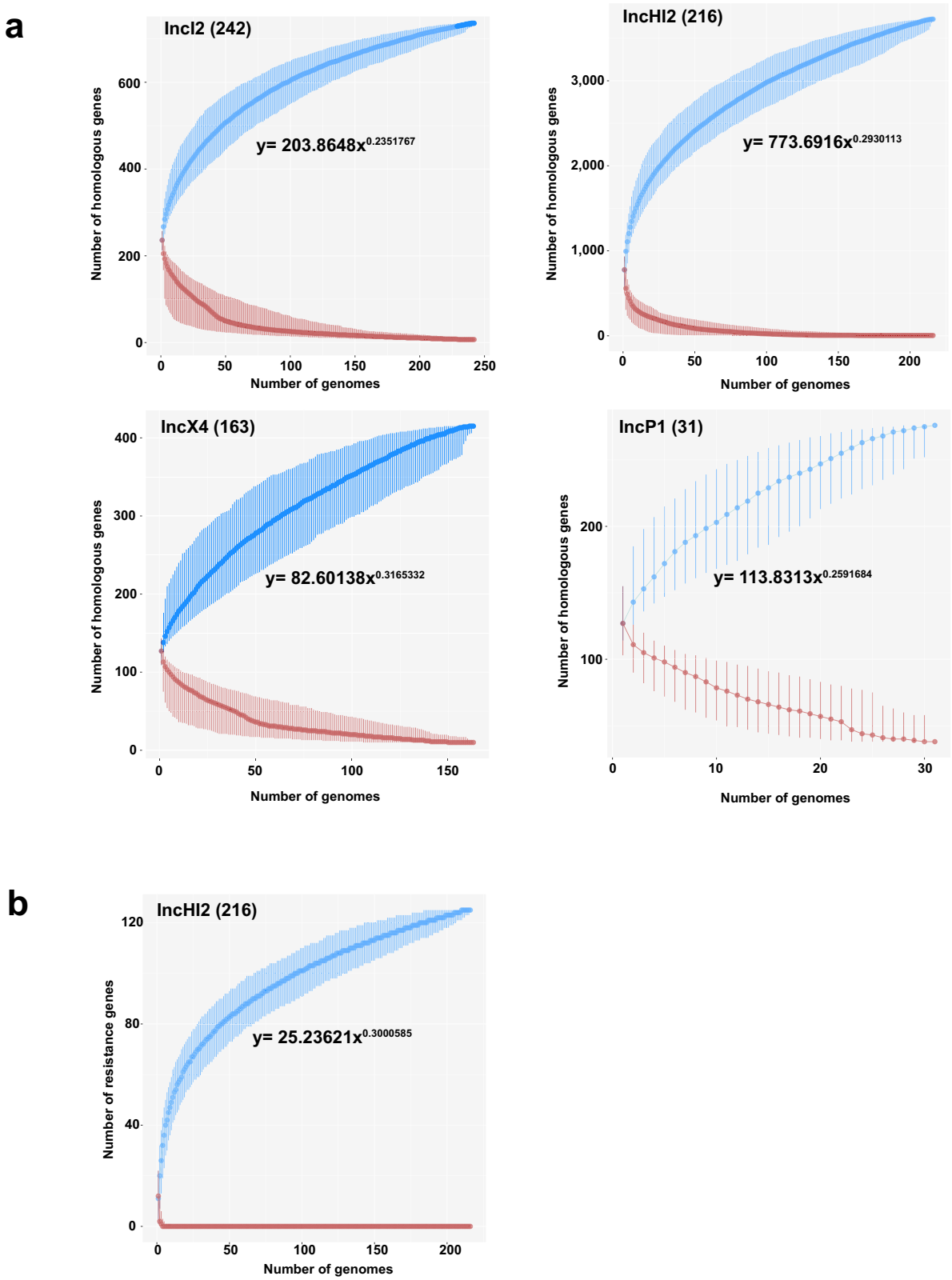

Fig. 4 | Accumulation curves for the pan/core-genomes/ resistance-genomes of *mcr*-carrying plasmids (pMCRs). a Accumulation curves for the pan/core genomes of pMCRs belonging to four Inc types. Blue and red lines represent the number of pan and core genes in sample combinations, respectively. The blue and red dots represent the median number of genes. Median lines fit the power law equation $y = kx^{\gamma}$, and $\gamma > 0$ indicated an open pan-genome. IncI2: $n = 242$; IncHI2: $n = 216$; IncX4: $n = 163$; IncP: $n = 31$. **b** Accumulation curves for the pan/core-resistance genome of IncHI2 pMCRs. Blue and red lines represent the number of pan and core-resistant genes in sample combinations, respectively. The blue and red dots represent the median number of genes. $\gamma > 0$ indicated an open pan-resistant genome.

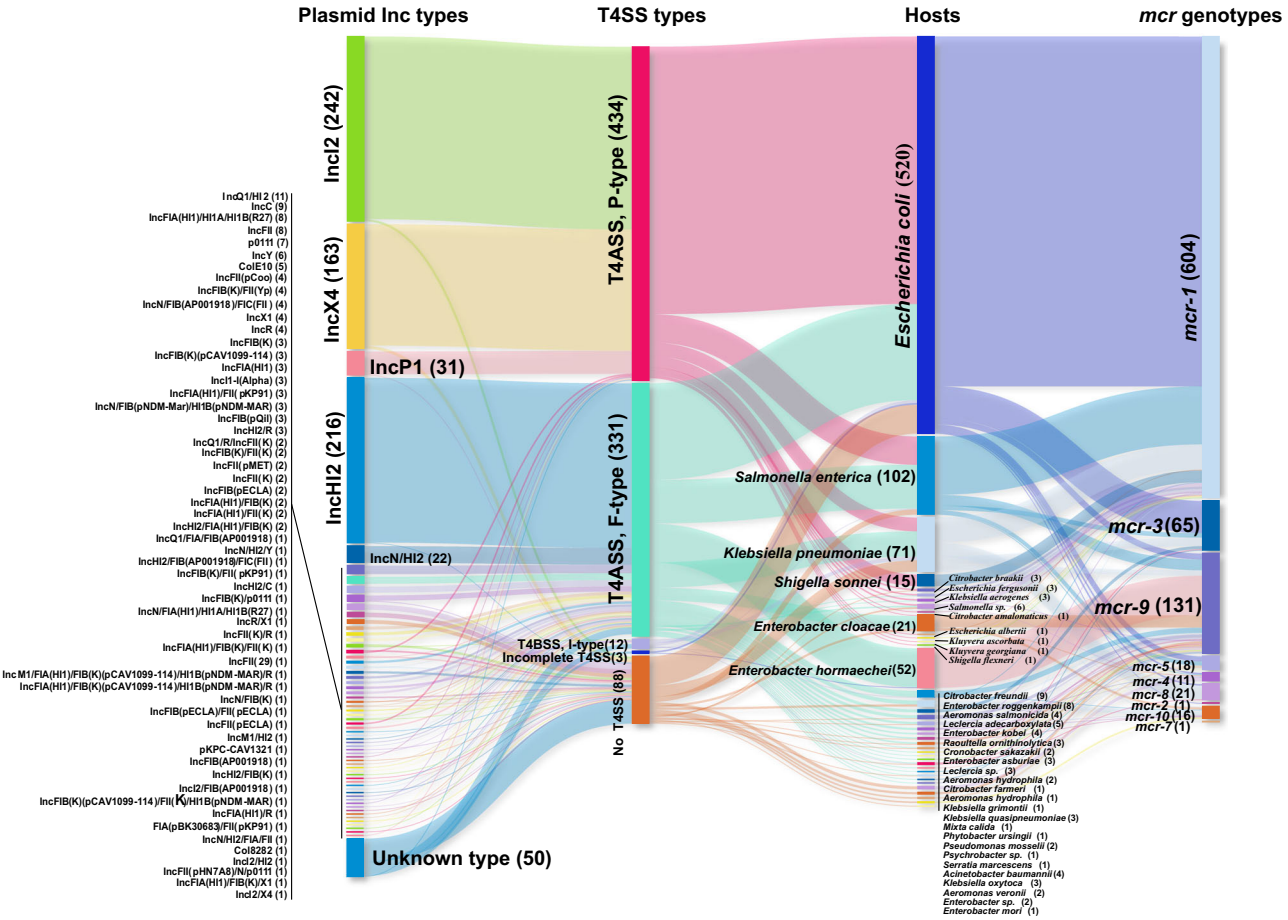

Fig. 5 | Correlation between T4SS types, plasmid replication types, bacterial hosts, and *mcr* genotypes. The Sankey diagram illustrates the corresponding relationships in the following order: plasmid replicon types to T4SS gene clusters, T4SS gene clusters to host bacteria, and host bacteria to the carried *mcr* gene types. Due to space limitations, the names of the 58 replicon types are labeled alongside the image. "Unknown type" means: no known plasmid replicon type was identified. "No T4SS" means: no known T4SS gene cluster was identified. The number of plasmids in each group is shown in parentheses. The data are provided in the Supplementary Data 1 (https://doi.org/10.5281/zenodo.14861845).

$T4SS_P$ is a complex multicomponent transmembrane structure. VirB2 and VirB5 are the major and minor subunits of the T pilus, respectively, and protein-protein interaction analysis suggests that VirB5 has cell-binding activity[31,36]. The function of T pilus in pMCR transfer was assessed using the deletion plasmids p841DEL*virB2*/ p402DEL*virB2* and p841DEL*virB5*/ p402DEL*virB5*. The deletion of VirB2 occurs between Lys2 and Lys96, covering 95 amino acids, while the deletion of VirB5 occurs between Asp3 and Leu212, covering 210 amino acids. Similar to T4SS absent plasmids, *virB2* deletion abolished plasmid transfer and bacterial conjugation, whereas *virB5* deletion significantly decreased transfer efficiency ($p < 0.0001$, $n = 9$) and maintained plasmid transfer at a low level in most conjugation pairs (Fig. 8). The absence of *virB5* decreased plasmid transfer approximately 115 and 58-fold in the *E. coli* and *K. pneumoniae* groups, respectively, and seven-fold in the *S.* Typhimurium group (Fig. 8b). Meanwhile, compared to plasmids with a single-gene deletion, the transfer rate of complementary plasmids significantly restored ($p < 0.0001$, $n = 9$, Fig. 8). Therefore, $T4SS_{P3}$ had an indispensable role in pMCR transfer. For T pilus, distinguished from the absolute dependence on VirB2, the dependence of conjugation on VirB5 varied across recipient species.

A crucial role for the T4SS gene cluster in the transfer of pMCR to the *E. coli* host in vivo

To further investigate the role of the T4SS gene cluster in the in vivo transfer of pMCRs, the mouse intestinal conjugation model was utilized to assess the transfer efficiency of the plasmid carrying the intact T4SS gene cluster, T4SS-deletion plasmid, and single-deletion plasmids of *virB2* and *virB5*. Each of the four plasmids was carried by J53, and after being mixed in equal proportions, they consisted of a consortium of donors. The donor consortium was then administered through gavage into the mouse intestine pre-colonized with the *E. coli*, *K. pneumoniae*, and *S.* Typhimurium recipients, respectively. In the *E. coli* conjugation group, the transfer efficiency of the wild-type plasmids ranged from 10^{-2} to 10^{-3}, while that of the *virB5*-absent plasmids was between 10^{-4} and 10^{-5}, representing a reduction of approximately 92-fold in p841GFP group (66-fold in p402GFP group) (Fig. 9). No transconjugants carrying T4SS-deletion plasmid and *virB2*-deletion plasmid were detected, indicating that these two plasmids also lack transferability in vivo. For *E. coli* recipients, the transfer trends of the four plasmids are generally consistent both in vivo and in vitro.

In contrast to the *E. coli* conjugative group in vivo, no transconjugant was obtained in the *K. pneumoniae* and *S.* Typhimurium conjugative groups. We then selected two other wild-type strains of each species as the recipients to repeat the conjugation experiments, but still, no transconjugant was obtained. Compared to the lower conjugation rate (approximately 10^{-5}) observed in the *S.* Typhimurium group, the transfer rate in the *K. pneumoniae* group was comparable to that of the *E. coli* group. It is generally believed that *K. pneumoniae* has an exceptional ability to acquire both exogenous antibiotic resistance genes and virulence factors[37], but the reason why we did not observe conjugation in the mouse gut model remains to be further investigated.

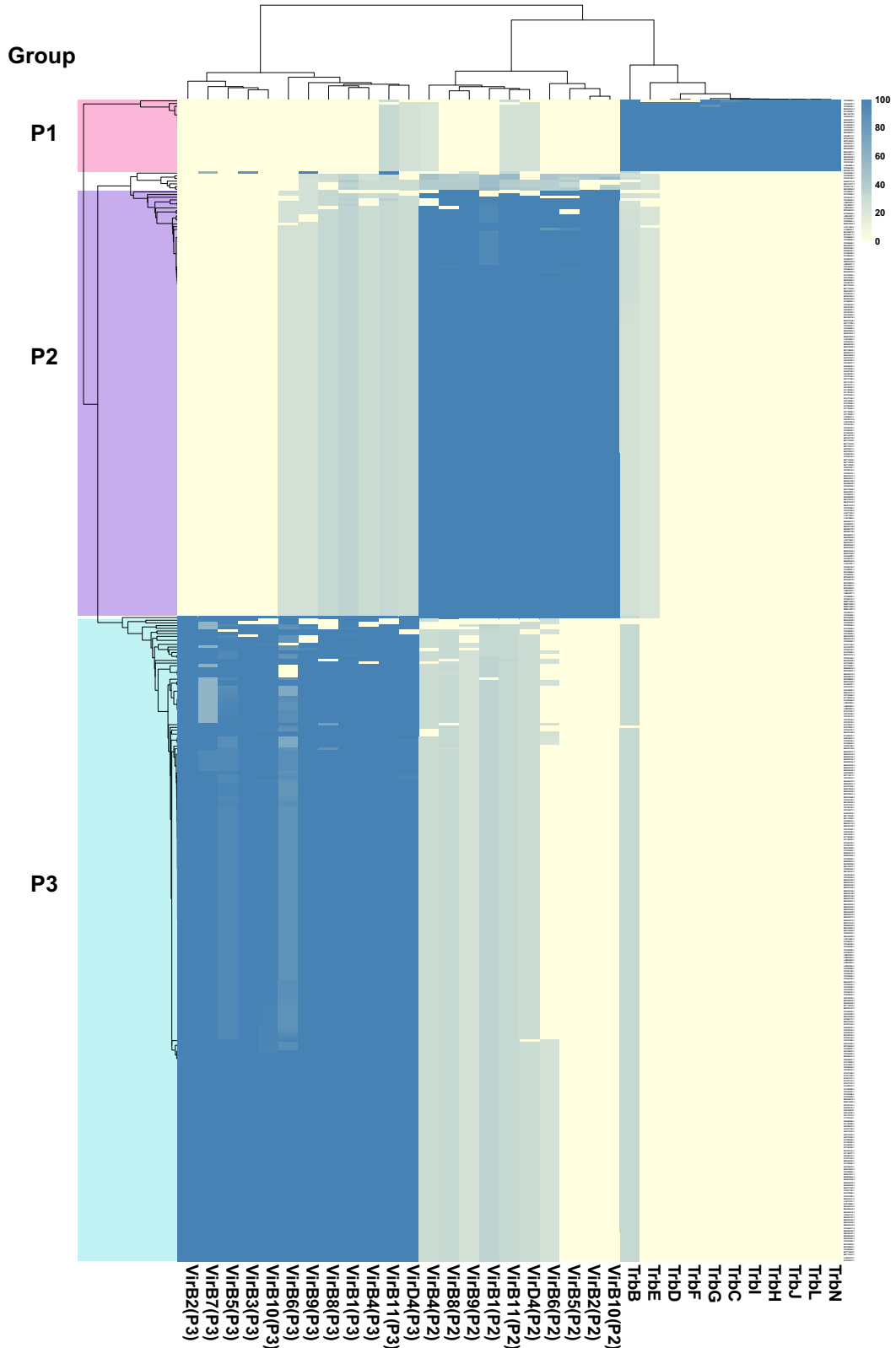

Fig. 6 | Homology analysis of amino acid sequences encoded by pMCRs carrying T4SS$_P$. A total of 434 plasmids were evaluated, and the amino acid sequences of 33 core genes from three T4SS gene clusters (MH522411.1(12), KX711707.1(10), MF489760.1(11)) served as references. Plasmids were divided into three groups based on sequence homology.

Diversity and structure prediction of VirB5 in T4SS$_{P3}$

Conjugative T4SSs must first produce a conjugative pilus, which contacts a recipient cell and serves as a conduit for DNA[30]. VirB5 forms the conjugative pilus and is located at the tip of the pilus[30]. VirB5 and VirB2 mediate cell-cell interactions between host and recipient[31,38–42]. A hypervariable region was located at the C-terminus of VirB5$_{P3}$ (Supplementary Fig. 9), and a 23-amino acid signal peptide was predicted at the N-terminus. The three-dimensional structure of mature

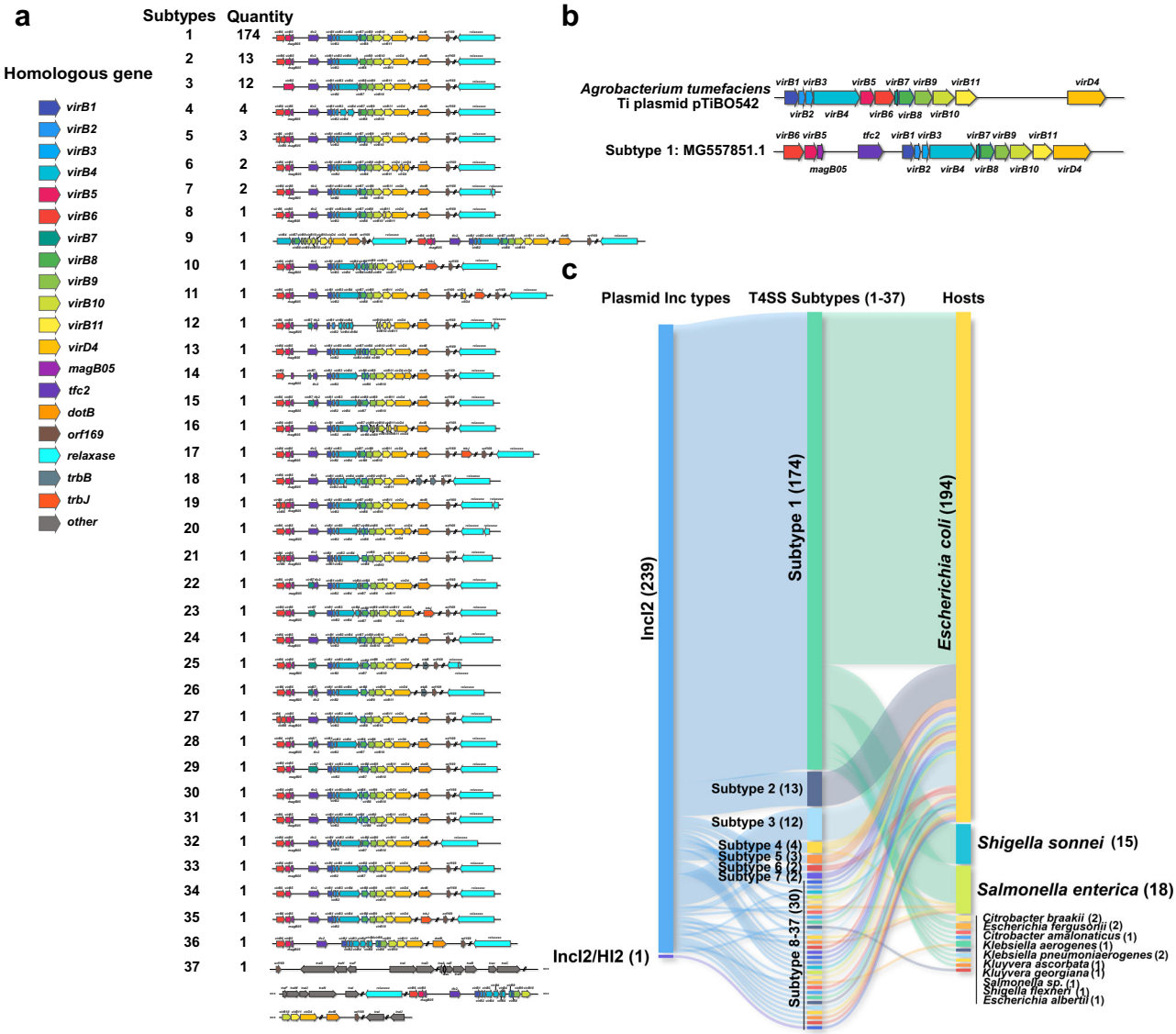

Fig. 7 | Structural diversity of T4SS$_{P3}$ and the relationship between T4SS subtypes, bacterial hosts, and plasmid replication types. a Gene structures of 37 T4SS subtypes in group P3. The regions in gray correspond to T4SS$_F$, and the regions in other colors correspond to T4SS$_P$. **b** T4SS gene cluster structure between T4SS$_{P3}$ and *Agrobacterium tumefaciens* Ti plasmid. The regions with the same color represent proteins of the same family. **c** Relationship between T4SS subtypes, bacterial hosts, and plasmid Inc types. The number of plasmids in each group is shown in parentheses. Subtypes 8 to 37 were annotated together because each had only one plasmid.

VirB5$_{P3}$ (NCBI Reference Sequence: WP_001425343.1) was predicted using Alphafold2, and sequence diversity was analyzed (Fig. 10a). The structure of VirB5$_{P3}$ was similar to homologs (TraC in pKM101 and TrwJ in pR388) crystallized as single proteins[36], but amino acid sequence identity was low (23.44% and 27.36%) (Supplementary Fig. 10). VirB5$_{P3}$ consisted of a three-helix bundle and a loose globular region (Fig. 10a).

The molecular weight of the native and denatured states of VirB5$_{P3}$ was 109.4 kDa and 21.9 kDa, respectively (Fig. 10b), suggesting that VirB5$_{P3}$ is a pentamer. The report of the T4SS$_{R388}$ crystal revealed the pentameric models of TrwJ (a homolog of VirB5 in pR388)[30], which was similar to the structure of VirB5$_{P3}$ predicted by AlphaFold2 (Fig. 10c and Supplementary Fig. 10). Pentamers were the most stable structure (Supplementary Fig. 11). However, in the pentameric form, VirB5$_{P3}$ appears to have undergone a conformational change compared with the monomer, and its N-terminal region was projected out in a manner reminiscent of pore-forming proteins (Fig. 10c). This structure may be required to interact with the membrane of the recipient cell[30].

Discussion

The spread of resistant plasmids is the primary cause of the rapid dissemination of bacterial resistance, and effectively inhibiting plasmid transfer is a key strategy for controlling resistance. The prevalence of pMCR plasmids reflects the global severe antibiotic resistance situation, leading to an increased clinical burden in the treatment of multidrug-resistant Gram-negative Enterobacteriaceae. Our previous research has reported the cross-host, cross-region transmission of pMCR, involving environmental, food, and human transmission chains, highlighting the risk of antibiotic resistance spread within a One Health context[43]. The study is also based on complete plasmid maps, which are indispensable in analyzing the co-carriage of resistance genes, evaluating sequence similarity, and plasmid tracing, areas where second-generation draft genomes fall short.

This study places greater emphasis on the genomic characteristics of pMCR and, using complete plasmid genomes, provides a clear illustration of the active genomic integration capacity of the IncHI2 type. This is reflected in the broad length range, key components of the fusion plasmids, and notable co-carriage of resistance genes (Supplementary Fig. 2).

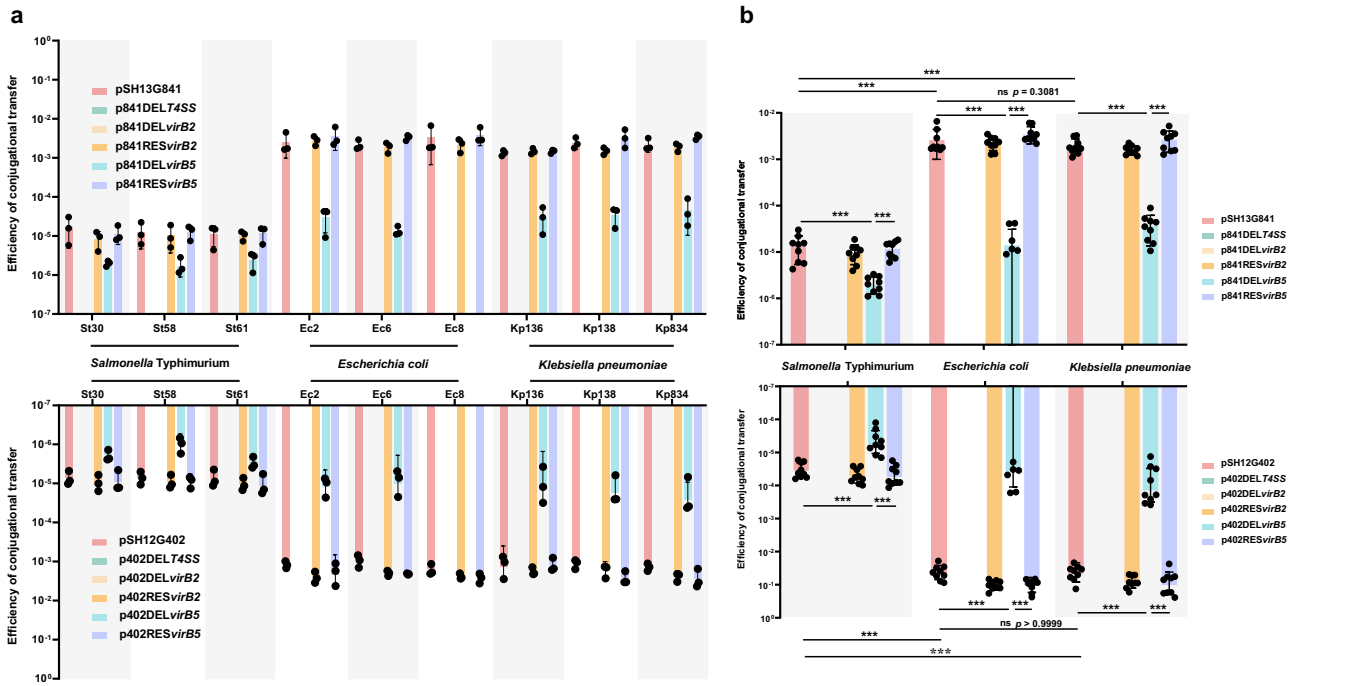

Fig. 8 | Transfer rates of pMCR (pSH13G841 and pSH12G402) and four types of T4SS gene cluster-associated absent plasmids to three Enterobacteriaceae species. a Plasmid transfer rates to nine recipients. St: *Salmonella* Typhimurium (3), Ec: *Escherichia coli* (3), Kp: *Klebsiella pneumoniae* (3). The experiments were repeated independently three times. **b** Plasmid transfer rates to three Enterobacteriaceae species. p841RESvirB2 and p841RESvirB5 are the corresponding gene recovery plasmids for p841DELvirB2 and p841DELvirB5, respectively, as in pSH12G402. pSH12G402 is the biological replicate of pSH13G841. ***represents *p-value* < 0.0001. Each experimental group was repeated three times. Each group contains three data points. Each black dot represents an individual data point. The Mean, SD, and N values are provided in Supplementary Data 4.

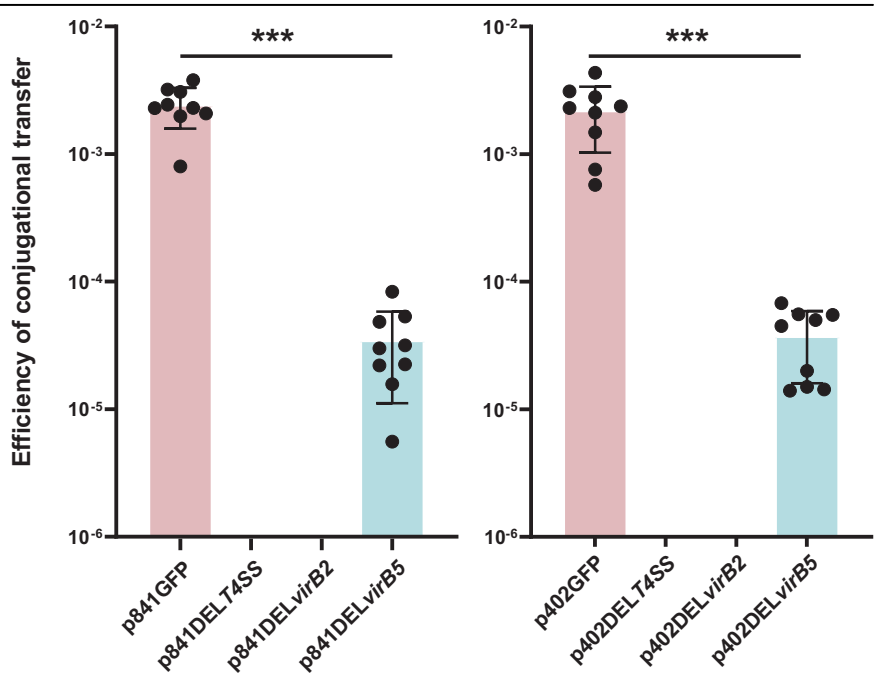

Fig. 9 | Competition conjugation experiment of pMCR-modified plasmids in *E. coli* in the mouse intestinal tract. The vertical axis is represented by the $\log_{10}$ value representing an individual data point. For each recipient conjugation group, nine mice were used as biological replicates. Conjugation efficiency is the ratio of transconjugants to recipient bacteria in feces. p841GFP: pSH13G841 carrying GFP; p841DEL*T4SS*: pSH13G841 with a deletion of the T4SS gene cluster; p841DEL*virB2*: pSH13G841 with a deletion of *virB2*; p841DEL*virB5*: pSH13G841 with a deletion of *virB5*. p402GFP is the biological replicate of p841GFP. Transconjugants carrying p841GFP or p402GFP were identified by observing fluorescent signals, and transconjugants carrying p841DEL*T4SS*/p402DEL*T4SS*, p841DEL*virB2*/p402DEL*virB2*, or p841DEL*virB5*/p402DEL*virB5* were confirmed by sequencing PCR products. Three mice were assigned to each recipient strain conjugation group, and the experiment was independently repeated three times. Each group contains nine data points. The Mean, SD, and N values are provided in Supplementary Data 4. "****" represents a *p-value* < 0.0001.

The fusion of multiple plasmid types means greater recruitment of ARGs and enhanced host adaptation, making IncHI2 more prone to resistance transmission. This may be attributed to its own mobile genetic elements, such as IS*26*[44]. One notable example is the detection of an IncHI2 pMCR-1 (MK673549.1) isolated from *Pseudomonas mosselii* within the order Pseudomonadales, suggesting that IncHI2-mediated *mcr-1* dissemination has expanded beyond the Enterobacteriales. The length distribution of IncI2 plasmids is concentrated, with a particularly low proportion of fusion plasmids involved, suggesting that its genome is more conserved. This type of pMCR has a high prevalence and is considered the best vector for the spread of *mcr-1*[18]. This may be attributed to its encoded plasmid copy number repressor (PcnR), which regulates plasmid copy number to balance the trade-off between plasmid dissemination and host adaptation[45]. An in vitro competitive experiment demonstrated that *E. coli*

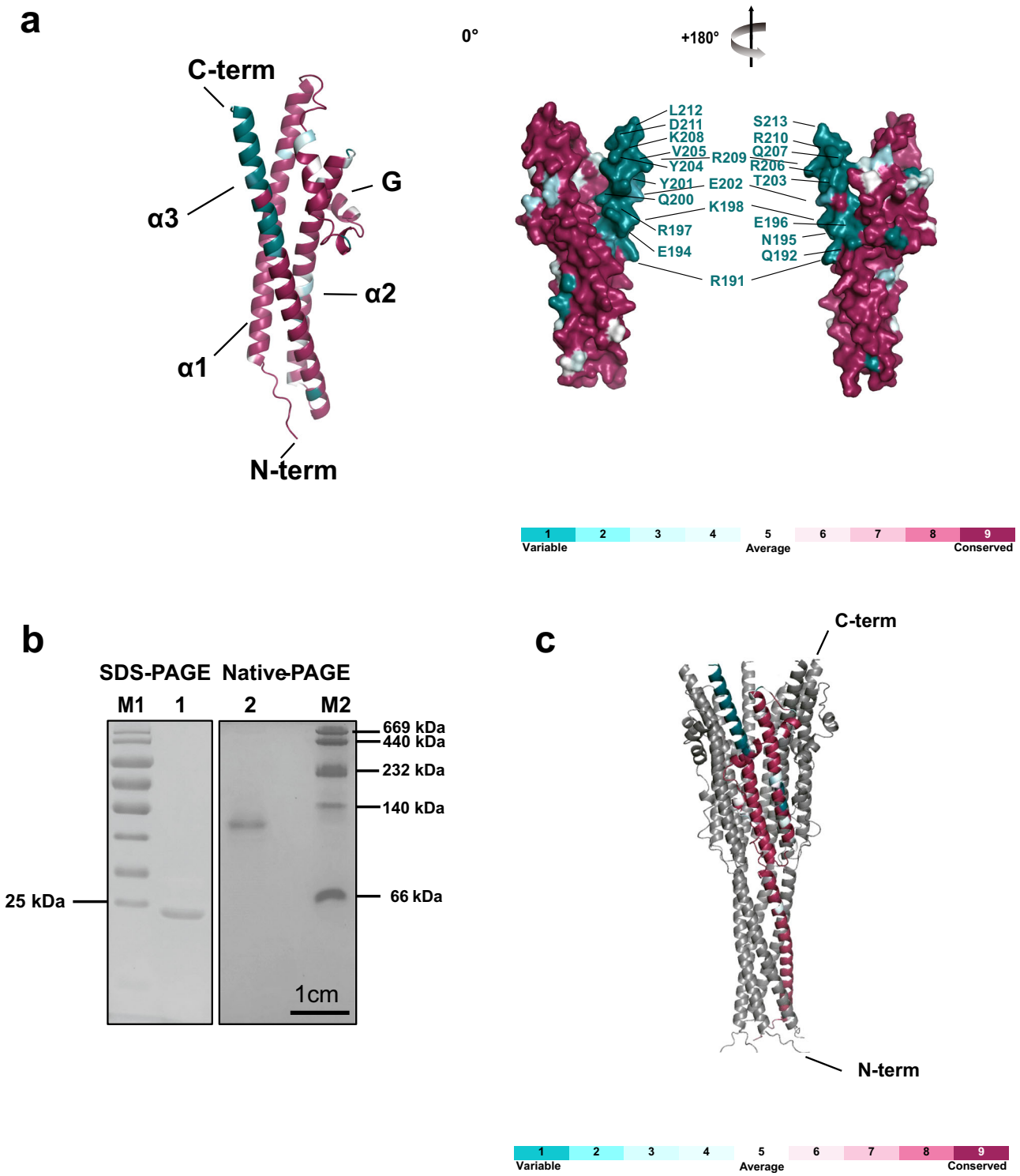

Fig. 10 | Structure prediction of the monomer and pentamer of VirB5$_{P3}$. **a** Structure prediction of the VirB5$_{P3}$ monomer and a hypervariable region at the C-terminus. G: globular region. The green text marks the residues of the hypervariable region. **b** Molecular weight of denatured and non-denatured VirB5$_{P3}$. The protein markers: M1: PageRuler Prestained Protein Ladder (Catalog No. 26616, Thermo Fisher Scientific); M2: HMW Native Marker (66–669) (Catalog No. 17-0445-01, GE). 1: Denatured VirB5$_{P3}$ monomer protein; 2: The pentameric VirB5$_{P3}$ protein in the non-denatured state. The results were repeated three times. The scale bar is 1 cm. The original gel images are provided in Supplementary Fig. 13. **c** Prediction of the pentameric structure of VirB5$_{P3}$. Sequence conservation is marked on only one chain of the pentamer. Sequence conservation gradually increases from green to purple. Conservation coloring was generated by the ConSurf Server, and the protein structure was displayed using PyMOL version 2.4.1.

hosts carrying IncI2 had a growth advantage over those carrying IncHI2 and IncX4 plasmids[46].

During the identification of T4SS gene clusters, significant diversity was observed in the composition of the T4SS$_F$ (results not shown), with frequent subunit duplications and inverted insertions. IncHI2 and most fusion plasmids exclusively harbor the T4SS$_F$, indicating that this diversity may result from the active recombination of these plasmids (Fig. 5). The correlation between different T4SS$_F$ subtypes and plasmid types is still

unclear, and the active recombination and integration capabilities increase difficulty to the study of gene cluster functions. In contrast, $T4SS_P$ carried by IncI2, IncX4, and IncP pMCRs exhibit strict conservation (Fig. 6). Sequence consistency clustering based on gene cluster subunits showed that $T4SS_P$ was divided into three distinct groups, corresponding to their respective plasmid replicon types. There were clear homology boundaries between the groups, with no shared components and low homology among subunits. Although $T4SS_{P2}$ and $T4SS_{P3}$ are both annotated as VirB/D4 types in *oriT*finder, they differ greatly in composition and homology. $T4SS_{P3}$ is a typical $T4SS_{A.\ tumefaciens}$-like gene cluster consisting of 12 subunits, while $T4SS_{P2}$ lacks the corresponding VirB3 and VirB7(Fig. 6). Taking the conserved VirB2 from both gene clusters ($VirB2_{MH298055.1}$ and $VirB2_{MH522411.1}$) as an example, the identity is only 19.5%, and Root Mean Squared Error (RMSD) of the predicted model is 8.75, indicating no structural similarity. The predicted pentameric structure of VirB5 in $T4SS_{P2}$ can no longer form the torch-like morphology of $VirB5_{P3}$ and $VirB5_{R388}$[25]. Hence, this study focuses on $T4SS_{P3}$, specifically carried by IncI2, as the preferred choice for investigating T4SS conjugation mechanisms due to its stable and classical gene cluster structure, as well as its high prevalence. The functional exploration of the highly diverse $T4SS_F$ and the other two $T4SS_P$ subtypes is not addressed in this study, which represents a limitation of our current research. We will gradually uncover this in future studies.

Quantitative conjugation experiments revealed the indispensable role of $T4SS_{P3}$ in the transfer of pMCRs to Enterobacteriaceae. The crystal structure shows that VirB2 forms the tubular structure of the conjugative pilus[25,30], contributing to the attachment and extension of VirB5. Its absence leading to the cessation of conjugation demonstrates the indispensability of the plasmid transfer conduit. In contrast, the absence of $VirB5_{P3}$ led to a significant decrease in the transfer rate, though not a complete loss. The most notable changes were observed in *the E. coli* and *K. pneumoniae* group. This suggests that the presence or absence of $VirB5_{P3}$ has a relatively specific impact on the transfer rate of IncI2 plasmids to *E. coli* and *K. pneumoniae* hosts. It can be speculated that VirB5, as an extracellular component initially contacting recipient bacteria, may contribute to the efficient transfer of pMCR-1 to *E. coli* and *K. pneumoniae* recipient strains. The molecular basis for this preference may be due to differences in membrane structures of the recipient bacteria or the adaptive cost of the plasmid in the host bacteria, which requires further investigation. It is worth noting that the bacterial density in vitro experiments is much higher than that in natural conjugation conditions, potentially leading to rationalized and exaggerated phenotypes. In the mouse model, transconjugants were observed solely in the *E. coli* group. All three Enterobacteriaceae can colonize the mouse intestines, but compared to the *E. coli* group, both the *S.* Typhimurium and *K. pneumoniae* groups showed pathological responses, including weight loss, lethargy, hair loss, and diarrhea, with the most pronounced symptoms observed in the *S.* Typhimurium group. We speculate that the host immune response may be one of the reasons interfering with conjugation. In addition, there may be differences in intestinal localization between recipient and donor bacteria, making it difficult to determine their opportunities for contact, and thus the conditions cannot be equated with those of in vitro experiments. Existing studies still cannot provide a clear explanation for this phenomenon, and further investigation is needed.

Although previous studies have revealed the crystal structure of the $T4SS_P$ carried by the R388 plasmid[25], the gene cluster arrangement and homology differ significantly from those of $T4SS_{P3}$ carried by IncI2. TrwJ, a homologous protein of $VirB5_{P3}$ in $T4SS_{R388}$, shares a similar pentameric structure with $VirB5_{P3}$[30], but only has 27.36% amino acid sequence identity (Supplementary Fig. 10). A hypervariable region is located at the C-terminus of $VirB5_{P3}$. In the pentameric structure, this hypervariable region is surrounded by an outward inverted conical shape, which may be a groove involved in protein interaction. The diversity of this region is strongly associated with $VirB6_{P3}$ (Supplementary Fig. 12), suggesting it serves as their interaction interface, a co-evolutionary relationship also observed in $T4SS_{R388}$[30]. In $T4SS_{P3}$, the biological implications of the co-evolution of *virB5* and *virB6* being separate from the main gene cluster warrant further investigation. Furthermore, the conserved N-terminal structure of $VirB5_{P3}$ presents a potential target for developing small-molecule inhibitors to suppress IncI2-type plasmid transfer.

In conclusion, this study used comparative genomics based on complete plasmid sequences to uncover the genetic background and transmission preferences of pMCRs. It highlights the multidrug resistance risks associated with major epidemic plasmid replicons. The study focused on the genetic diversity and function of the $T4SS_{P3}$ exclusively carried by the IncI2 plasmids, observed its preferential transfer to *E. coli*, and clarified the key biological roles of pilus subunits. This provides more ideas for the effective prevention and control of polymyxin resistance.

Methods

Bacterial strains, plasmids, primers, and culture conditions

The bacteria and plasmids used in this study are listed in Supplementary Table 1 and Supplementary Table 2. The plasmid pSH13G841 and pSH12G402 are stored in our laboratory. The donor bacterial strain in conjugation was *E. coli* J53, and the recipient strains were *S.* Typhimurium, *E. coli*, and *K. pneumoniae* without colistin resistance and IncI2 plasmids. Unless otherwise noted, these strains were grown in Luria-Bertani (LB) medium or LB plates containing 1.5% agar (LBA) at 37 °C. The final concentration of the antibiotics was 100 μg mL^{-1} (streptomycin and NaN_3), 4 μg mL^{-1} (polymyxin B), and 10 μg mL^{-1} (chloramphenicol). Primers used in this study are shown in Supplementary Table 3.

Collection of pMCRs with complete genome sequences

pMCRs were collected by performing a homology search against *mcr* genes in the NCBI database (as of April 2021). We collected sequences of 10 *mcr* allelic genes and used them as input information for Blastn (https://blast.ncbi.nlm.nih.gov/Blast.cgi?PROGRAM=blastn&PAGE_TYPE=BlastSearch&LINK_LOC=blasthome) comparisons to capture plasmid genomes carrying the *mcr* genes. Remove duplicate identifiers from the Blast results of various allelic genes based on the GenBank accession number of the genome, and retain only plasmid genomes with the sample names containing "complete genome" or "complete sequence." After genome deduplication and exclusion of artificially constructed engineered plasmids, we obtained 868 genomes of pMCRs, of which 37 were submitted by our laboratory[35]. The GenBank accession numbers for the genomes are recorded in Supplementary Data 2. Sample information of 868 pMCRs is recorded in Supplementary Data 3.

Identification of Inc plasmids and T4SS types

Inc types and T4SS subtypes were identified using PlasmidFinder version 2.1 of the Center for Genomic Epidemiology (https://cge.food.dtu.dk/services/PlasmidFinder/)[47] and *oriT*finder (https://bioinfo-mml.sjtu.edu.cn/oriTfinder/)[48].

Homology analysis of T4SS gene clusters

The amino acid sequences of 33 T4SS core genes were used as references (Supplementary Data 1). The genes in 434 plasmids carrying $T4SS_P$ were predicted using Prodigal version 2.6.3. Translate the gene sequence into an amino acid sequence and perform a BLAST search against the reference sequence. Data were represented as a two-dimensional matrix (plasmid vs. reference genes). The threshold for homologous protein is set with query coverage >60%[49,50] and e-value < 0.00001[50]. When a homologous sequence in the database was identified on the plasmid, a value of 1 was input into the corresponding position in the matrix. When homologous genes were not found, a value of 0 was entered into the matrix. Hierarchical clustering and heatmap were performed using the pheatmap package in R (version 4.2.1) (https://github.com/lizhe19900504/code).

Pan and core-genome analysis

The genes of the four Inc types of pMCR were predicted using Prokka[51], and the annotation files were output in gff3 format. Using the annotation files as input, pan-genome analysis was performed using Roary[52]. The core genes

were determined based on the acquisition and loss status of each gene in the Roary results file. The size of core genes or pan genes was estimated by a random combination of genomes with a specified number. Draw curves of the core or pan-genome by connecting the median number of reference genes aligned for each randomly selected combination of genomes. Pan and core-genome curves were calculated as the least-squares fit of the power law $y = kx^{\gamma}$ to medians. The analysis of pan and core genes of antibiotic resistance genes is the same as this method.

Measurement of bacterial growth

Bacterial cells were grown in LB medium overnight, diluted 100-fold in LB medium, and grown to logarithmic phase (OD_{600} = 0.5–0.8). Then, 200 µL of the culture was added to a 100-well plate. Bacterial growth was measured kinetically by continuously monitoring optical density every 30 min for 24 h using an automated turbidimeter (Bioscreen C, Finland). The experiments were performed in sextuplicate.

Editing of plasmid genomes

Gene editing (deletion or restoration) was achieved using the suicide plasmid-mediated homologous recombination technique[53]. The suicide plasmid selected was the pWM91CM, derived from the pWM91[54] and modified by inserting the promoter and ORF of *cat* gene at the *BamHI* and *XhoI* sites. The 1 kb upstream and downstream regions of the target gene were amplified through PCR using pSH13G841 or pSH12G402 as a template, then combined by overlap PCR and inserted into the suicide plasmid. The cloned plasmid in *E. coli* SM10 λpir was transformed into *E. coli* J53 containing pSH13G841 or pSH12G402 by conjugation. The transformants grown on salt-free sucrose plates with chloramphenicol-sensitive are target clones. The deletion was confirmed through PCR screening and sequencing of the 2 kb amplicon produced by overlapping primers. PCR results were validated through sequencing. The location of the T4SS gene cluster deletion spans from the 9th base pair of the *virB1* ORF to the 1941st base pair of *virD4*, with a deletion length of 9446 bp, including *virB1*, *B2*, *B3*, *B4*, *B7*, *B8*, *B9*, *B10*, *B11*, and *D4*.

The principle of gene restoration is similar to that of deletion, with the difference being the integration of the insertion fragment by overlapping between the upstream and downstream homologous arms and then integrating into the corresponding gene locus through homologous recombination. In constructing pSH13G841GFP, pSH13G841RESVirB5, and pSH12G402RESVirB5, the integration fragments were designed with the PLtetO-1 promoter linked to the corresponding open reading frame (ORF) (*gfp* or *virB5* gene). However, in the construction of pSH13G841RESVirB2 and pSH12G402RESVirB2, the integration fragment is designed with the original gene cluster promoter linked to the ORF of *virB2*. The plasmids and primers used in this experiment are listed in Supplementary Tables 2 and 3.

Generation of donor strains

S. Typhimurium strains carrying either pSH13G841 or pSH12G402 are used as donor strains, with *E. coli* J53 as the recipient strain in conjugation. Conjugative parents were mixed and cultured on LBA plates. Transconjugants were selected on LB agar containing 4 µg mL^{-1} polymyxin B and 100 µg mL^{-1} NaN_3 at 37 °C for 20 h. Transconjugants were confirmed by PCR.

Assessment of conjugation efficiency

For each conjugation experiment, bacterial suspensions of donor and recipient at OD600 of 0.5 (approximately 4×10^8 CFU/mL) were each aliquoted at 500 µL and mixed in a 1.5 mL tube. The mixed cultures were grown statically at 37 °C for 2 h. The supernatant was replaced with 100 µl PBS. Bacterial suspensions were transferred to the center of LB plates covered with a 0.45 mm filter membrane and cultured at 37 °C overnight. Cultures were diluted in a ten-fold gradient in PBS and 10 µL drops on polymyxin B, streptomycin, and both dual-resistant plates for colony count. Positive transformants were screened by real-time PCR targeting the *mcr-1* gene. Plasmid transfer rates (γ) were calculated as $\gamma = \log_{10}\left(\frac{T}{\sqrt{D*R}}\right)$, where *D*, *R*, and *T* represent the number of donor, recipient, and transformed colonies per milliliter, respectively[55].

Competitive plasmids conjugation in vivo

The mouse intestinal conjugation model was adapted from the study by Kevin Neil et al.[56]. In the in vivo plasmid transfer experiments, 6-week-old female C57BL/6 N mice were used. These mice carried a complex specified pathogen-free (SPF) microbiota. Three mice were assigned to each recipient strain conjugation group, and the experiment was independently repeated three times. The experiment has three phases, i.e., clearance with antibiotics, recipient colonization, and donor colonization for conjugative transfer. Specifically, animals were pretreated with 25 mg streptomycin and 15 mg ampicillin orally to allow for robust colonization of the recipient. Antibiotic gavage was administered for two consecutive days to enhance the clearance effect, and daily confirmation of the clearance effect was conducted through 10-fold gradient dilution plating of feces. Simultaneously, 5 mg mL^{-1} of both streptomycin and ampicillin were added to the drinking water at final concentrations. Recipients (*E. coli* strain Ec6) were cultivated overnight at 37 °C in LB containing 100 µg mL^{-1} streptomycin, and then cultured (1:20 dilution before culture) for 4 h at 37 °C in LB without antibiotics, washed with sterile PBS, and 2×10^8 CFU were introduced into mice via oral gavage. The recipient bacteria were continuously administered via gastric gavage for two days, followed by consecutive collection of feces for the next two days to assess colonization through gradient dilution, and the drinking water was replaced with antibiotic-free distilled water. The pre-colonization data for the recipient strains are provided in Supplementary Data 1 (https://doi.org/10.5281/zenodo.14861845). The conjugation donors were mixed using four *E. coli* J53 recombinant strains, each carrying one of the following plasmids: p841GFP (p402GFP), p841DEL*T4SS* (p402DEL*T4SS*), p841DEL*virB2* (p402DEL*virB2*), and p841DEL*virB5*(p402DEL*virB5*), respectively. The preparation method for each donor was the same as that of the recipients, and the inoculation dose was 5×10^7 CFU for each. Feces were collected the next day, subjected to a 10-fold gradient dilution, and plated on corresponding antibiotic resistance plates (colistin 4 µg mL^{-1}, streptomycin 100 µg mL^{-1}) for counting. Through fluorescence microscopy observation, colonies exhibiting green fluorescence upon excitation were confirmed to be wild-type plasmid conjugants, while the remaining colonies had their plasmid types confirmed through PCR. The conjugation efficiency was calculated as the percentage of transconjugants among the donor bacteria. Each mouse was housed individually, with three mice per group, repeated three times. All animal experiments in this study were conducted in accordance with the relevant animal ethics guidelines. The use of animals in this study was approved by the Ethics Committee of the National Institute for Communicable Disease Control and Prevention, Chinese Center for Disease Control and Prevention (license: 2023-046).

Expression, purification, and identification of the VirB5 protein

The gene sequence encoding the mature VirB5 protein was inserted in the pET15b vector and transformed into *E. coli* BL21 cells. The expression of the protein was induced with 1 mM isopropyl-b-D-thiogalactopyranoside (IPTG) for 4 h in LB liquid medium at 37 °C. The bacterial pellet was resuspended in binding buffer (15 mM Tris-HCl, 500 mM NaCl, pH 8.0) at a dilution of 1:10. The suspension was sonicated for 15 min and centrifuged (13,000 rpm, 30 min), and the target protein in the supernatant was purified by Ni-NTA affinity chromatography at 4 °C. The column was washed and eluted with washing buffer (binding buffer containing 20 mM imidazole pH 8.0) and elution buffer (binding buffer containing 250 mM imidazole pH 8.0), respectively. Protein concentration was measured using the Pierce BCA Protein Assay Kit (Catalog No. 23225). The molecular weight of monomers and native protein was determined by 12% SDS-PAGE and 10% native PAGE. The protein markers used in electrophoresis were PageRuler Prestained Protein Ladder (Catalog No. 26616, Thermo Fisher Scientific) and HMW Native Marker (66–669) (Catalog No. 17-0445-01, GE), respectively. The results were repeated three times.

Multiple sequence alignment, sequence homology analysis, and protein structure prediction

Multiple sequence alignments were performed using ClustalX version 2.1. The signal peptide of VirB5 was predicted using SignalP version 5.0[57]. The structure of VirB5 (24–213 aa) was predicted using AlphaFold2[58]. The best prediction model was chosen based on the alignment error, and the stereochemical quality of protein structures was assessed using SAVES. The structural model and multiple sequence alignments were uploaded to the ConSurf Server (https://consurf.tau.ac.il/)[59]. The results were displayed using PyMOL version 2.4.1.

Statistics and reproducibility

All statistical analyses in this study were performed using GraphPad Prism 9.0 (San Diego, CA). For the two-sample unpaired t-test, two-tailed *p*-value and 95% confidence interval were selected. If the data variance is unequal, Welch's correction can be applied. If the data does not follow a normal distribution, the Mann-Whitney test, a non-parametric test, can be used. Pearson correlation coefficients between T4SS protein elements were calculated by identity values of plasmid sequences with reference sequences. $P < 0.0001$ was considered statistically significant. Repeatability is described as follows:

Growth rate comparison of recipient strains: For each type of recipient strain, we selected three non-clonal strains and from each strain, six single-colony isolates were chosen. Each single-colony isolate was tested with three biological replicates, and the average value from each experiment was used as the final result. This design ensures that the results represent the biological variation of the recipient strains while minimizing biases from individual clones. The choice of 6 single-clone isolates provides a balance between statistical power and experimental feasibility, allowing us to capture the growth differences between strains and provide reliable statistical analysis. This sample size design is consistent with common practices in microbiological studies for assessing growth rate differences.

In vitro plasmid conjugation efficiency assessment: Recipient Strain Selection: For each recipient strain group, three non-clonal strains were selected. Each single-clone isolate was tested with three biological replicates (with the average of each experiment used as the final value). This design minimizes the effect of clonal variation and controls experimental errors through technical repeats. The three independent replicates ensure that the results are reliable and reproducible. Two IncI2 plasmids and their corresponding gene deletion constructs were selected for evaluating plasmid transfer efficiency. Using two different plasmids as biological replicates helps to avoid biases associated with a single plasmid and enhances the robustness and generalizability of the results. These biological replicates allow for an assessment of how different plasmid types affect conjugation efficiency.

The selected sample size (three non-clonal strains and three independent experimental replicates) meets the typical experimental design requirements in microbiology. This allows for reliable detection of transfer efficiency differences and ensures that the experimental results are statistically significant.

In vivo conjugation experiment: In the in vivo experiments, we selected one recipient strain per conjugation group, with three mice used as biological replicates. This sample size effectively considers biological variation in the mouse model while adhering to ethical guidelines. Three independent experiments were conducted to ensure the reproducibility of the results and reduce inter-experimental variability. The choice of three mice per biological replicate is a common practice in animal experiments, as this sample size is sufficient to detect significant effects while minimizing the use of animals. The Mean, SD, and N values are provided in Supplementary Data 4.

Reporting summary

Further information on research design is available in the Nature Portfolio Reporting Summary linked to this article.

Data availability

All data needed to evaluate the conclusions in the paper are present in the main text and/or the Supplementary Materials. The original data for the figures are provided in Supplementary Data 1. The GenBank accession numbers and sample information of *mcr*-carrying plasmids, as well as the Mean, SD, and N values in Figs. 8 and 9, are provided in Supplementary Data 2–4. Supplementary Data 1–4 are stored in the Zenodo database (https://doi.org/10.5281/zenodo.14861845). The original gels for SDS-PAGE and Native PAGE in Fig. 10b are provided as Supplementary Fig. 13 in the Supplementary Information. Some of the strains and plasmids used in this study are preserved in our laboratory. Please contact us if you wish to obtain them. Correspondence and requests for materials should be addressed to X.L. (luxin@icdc.cn) and B.K. (kanbiao@icdc.cn).

Received: 9 May 2024; Accepted: 14 February 2025;
Published online: 01 March 2025

References

1. van Duin, D. & Paterson, D. L. Multidrug-resistant bacteria in the community: an update. *Infect. Dis. Clin. North Am.* **34**, 709–722 (2020).
2. Gregoire, N., Aranzana-Climent, V., Magreault, S., Marchand, S. & Couet, W. Clinical pharmacokinetics and pharmacodynamics of colistin. *Clin. Pharmacokinet.* **56**, 1441–1460 (2017).
3. Liu, Y. Y. et al. Emergence of plasmid-mediated colistin resistance mechanism MCR-1 in animals and human beings in China: a microbiological and molecular biological study. *Lancet Infect. Dis.* **16**, 161–168 (2016).
4. Carattoli, A. Plasmids and the spread of resistance. *Int J. Med. Microbiol.* **303**, 298–304 (2013).
5. Behzadi, P. et al. Editorial: current perspectives on Pseudomonas aeruginosa: epidemiology, virulence and contemporary strategies to combat multidrug-resistant (MDR) pathogens. *Front. Microbiol.* **13**, 975616 (2022).
6. Olaitan, A. O., Morand, S. & Rolain, J. M. Mechanisms of polymyxin resistance: acquired and intrinsic resistance in bacteria. *Front. Microbiol.* **5**, 643 (2014).
7. Bialvaei, A. Z. & Samadi Kafil, H. Colistin, mechanisms and prevalence of resistance. *Curr. Med. Res. Opin.* **31**, 707–721 (2015).
8. Rhouma, M., Beaudry, F., Theriault, W. & Letellier, A. Colistin in pig production: chemistry, mechanism of antibacterial action, microbial resistance emergence, and one health perspectives. *Front. Microbiol.* **7**, 1789 (2016).
9. Nang, S. C., Li, J. & Velkov, T. The rise and spread of *mcr* plasmid-mediated polymyxin resistance. *Crit. Rev. Microbiol.* **45**, 131–161 (2019).
10. Elbediwi, M. et al. Global burden of colistin-resistant bacteria: mobilized colistin resistance genes study (1980-2018). *Microorganisms* https://doi.org/10.3390/microorganisms7100461 (2019).
11. Xiaomin, S. et al. Global impact of *mcr-1*-positive Enterobacteriaceae bacteria on "one health". *Crit. Rev. Microbiol.* **46**, 565–577 (2020).
12. Du, H., Chen, L., Tang, Y. W. & Kreiswirth, B. N. Emergence of the *mcr-1* colistin resistance gene in carbapenem-resistant *Enterobacteriaceae*. *Lancet Infect. Dis.* **16**, 287–288 (2016).
13. Yao, X., Doi, Y., Zeng, L., Lv, L. & Liu, J. H. Carbapenem-resistant and colistin-resistant *Escherichia coli* co-producing NDM-9 and MCR-1. *Lancet Infect. Dis.* **16**, 288–289 (2016).
14. Falgenhauer, L. et al. Colistin resistance gene *mcr-1* in extended-spectrum beta-lactamase-producing and carbapenemase-producing Gram-negative bacteria in Germany. *Lancet Infect. Dis.* **16**, 282–283 (2016).
15. Haenni, M. et al. Co-occurrence of extended spectrum beta lactamase and MCR-1 encoding genes on plasmids. *Lancet Infect. Dis.* **16**, 281–282 (2016).

16. Liu, J. H. et al. Plasmid-mediated colistin-resistance genes: *mcr*. *Trends Microbiol.* **32**, 365–378 (2024).
17. Jangir, P. K. et al. The evolution of colistin resistance increases bacterial resistance to host antimicrobial peptides and virulence. *eLife* https://doi.org/10.7554/eLife.84395 (2023).
18. Wang, R. et al. The global distribution and spread of the mobilized colistin resistance gene *mcr-1*. *Nat. Commun.* **9**, 1179 (2018).
19. Christie, P. J. The mosaic type IV secretion systems. *EcoSal Plus* https://doi.org/10.1128/ecosalplus.ESP-0020-2015 (2016).
20. Baron, C. From bioremediation to biowarfare: on the impact and mechanism of type IV secretion systems. *FEMS Microbiol. Lett.* **253**, 163–170 (2005).
21. Christie, P. J., Atmakuri, K., Krishnamoorthy, V., Jakubowski, S. & Cascales, E. Biogenesis, architecture, and function of bacterial type IV secretion systems. *Annu. Rev. Microbiol.* **59**, 451–485 (2005).
22. Christie, P. J., Gomez Valero, L. & Buchrieser, C. Biological diversity and evolution of type IV secretion systems. *Curr. Top. Microbiol. Immunol.* **413**, 1–30 (2017).
23. Chandran Darbari, V. & Waksman, G. Structural biology of bacterial type IV secretion systems. *Annu. Rev. Biochem.* **84**, 603–629 (2015).
24. Nagai, H. & Kubori, T. Type IVB secretion systems of legionella and other Gram-negative bacteria. *Front. Microbiol.* **2**, 136 (2011).
25. Costa, T. R. D., Patkowski, J. B., Mace, K., Christie, P. J. & Waksman, G. Structural and functional diversity of type IV secretion systems. *Nat. Rev. Microbiol.* **22**, 170–185 (2024).
26. Fronzes, R. et al. Structure of a type IV secretion system core complex. *Science* **323**, 266–268 (2009).
27. Gordon, J. E. et al. Use of chimeric type IV secretion systems to define contributions of outer membrane subassemblies for contact-dependent translocation. *Mol. Microbiol.* **105**, 273–293 (2017).
28. Low, H. H. et al. Structure of a type IV secretion system. *Nature* **508**, 550–553 (2014).
29. Ripoll-Rozada, J., Zunzunegui, S., de la Cruz, F., Arechaga, I. & Cabezon, E. Functional interactions of VirB11 traffic ATPases with VirB4 and VirD4 molecular motors in type IV secretion systems. *J. Bacteriol.* **195**, 4195–4201 (2013).
30. Mace, K. et al. Cryo-EM structure of a type IV secretion system. *Nature* **607**, 191–196 (2022).
31. Aly, K. A. & Baron, C. The VirB5 protein localizes to the T-pilus tips in *Agrobacterium tumefaciens*. *Microbiology***153**, 3766–3775 (2007).
32. Kamathewatta, K. et al. Colonization of a hand washing sink in a veterinary hospital by an *Enterobacter hormaechei* strain carrying multiple resistances to high importance antimicrobials. *Antimicrob. Resist. Infect. Control* **9**, 163 (2020).
33. Park, S. C., Lee, K., Kim, Y. O., Won, S. & Chun, J. Large-Scale Genomics Reveals the Genetic Characteristics of Seven Species and Importance of Phylogenetic Distance for Estimating Pan-Genome Size. *Front Microbiol* **10**, 834 (2019).
34. Tettelin, H., Riley, D., Cattuto, C. & Medini, D. Comparative genomics: the bacterial pan-genome. *Curr. Opin. Microbiol.* **11**, 472–477 (2008).
35. Lu, X. et al. Epidemiologic and genomic insights on *mcr-1*-harbouring *Salmonella* from diarrhoeal outpatients in Shanghai, China, 2006-2016. *EBioMedicine* **42**, 133–144 (2019).
36. Yeo, H. J., Yuan, Q., Beck, M. R., Baron, C. & Waksman, G. Structural and functional characterization of the VirB5 protein from the type IV secretion system encoded by the conjugative plasmid pKM101. *Proc. Natl Acad. Sci. USA* **100**, 15947–15952 (2003).
37. Yang, X., Dong, N., Chan, E. W., Zhang, R. & Chen, S. Carbapenem Resistance-Encoding and Virulence-Encoding Conjugative Plasmids in *Klebsiella pneumoniae*. *Trends Microbiol.* **29**, 65–83 (2021).
38. Backert, S., Fronzes, R. & Waksman, G. VirB2 and VirB5 proteins: specialized adhesins in bacterial type-IV secretion systems? *Trends Microbiol.* **16**, 409–413 (2008).
39. Hwang, H. H. & Gelvin, S. B. Plant proteins that interact with VirB2, the *Agrobacterium tumefaciens* pilin protein, mediate plant transformation. *Plant Cell* **16**, 3148–3167 (2004).
40. Aguilar, J., Cameron, T. A., Zupan, J. & Zambryski, P. Membrane and core periplasmic *Agrobacterium tumefaciens* virulence type IV secretion system components localize to multiple sites around the bacterial perimeter during lateral attachment to plant cells. *mBio* **2**, e00218–00211 (2011).
41. Andrzejewska, J. et al. Characterization of the pilin ortholog of the *Helicobacter pylori* type IV cag pathogenicity apparatus, a surface-associated protein expressed during infection. *J. Bacteriol.* **188**, 5865–5877 (2006).
42. Conradi, J. et al. An RGD helper sequence in CagL of Helicobacter pylori assists in interactions with integrins and injection of CagA. *Front. Cell Infect. Microbiol.* **2**, 70 (2012).
43. Li, Z., Li, Z., Peng, Y., Lu, X. & Kan, B. Trans-regional and cross-host spread of mcr-carrying plasmids revealed by complete plasmid sequences - 44 countries, 1998-2020. *China CDC Wkly* **4**, 242–248 (2022).
44. Fang, L. X. et al. High genetic plasticity in multidrug-resistant sequence type 3-IncHI2 plasmids revealed by sequence comparison and phylogenetic analysis. *Antimicrob. Agents Chemother.* https://doi.org/10.1128/AAC.02068-17 (2018).
45. Yang, J. et al. A ProQ/FinO family protein involved in plasmid copy number control favours fitness of bacteria carrying mcr-1-bearing IncI2 plasmids. *Nucleic Acids Res.* **49**, 3981–3996 (2021).
46. Wu, R. et al. Fitness advantage of mcr-1-bearing IncI2 and IncX4 plasmids in vitro. *Front. Microbiol.* **9**, 331 (2018).
47. Carattoli, A. & Hasman, H. PlasmidFinder and in silico pMLST: identification and typing of plasmid replicons in whole-genome sequencing (WGS). *Methods Mol. Biol.* **2075**, 285–294 (2020).
48. Li, X. et al. oriTfinder: a web-based tool for the identification of origin of transfers in DNA sequences of bacterial mobile genetic elements. *Nucleic Acids Res.* **46**, W229–W234 (2018).
49. Kourelis, J. et al. A homology-guided, genome-based proteome for improved proteomics in the alloploid Nicotiana benthamiana. *BMC Genomics* **20**, 722 (2019).
50. Salvetti, E., Campedelli, I., Larini, I., Conedera, G. & Torriani, S. Exploring antibiotic resistance diversity in Leuconostoc spp. by a genome-based approach: focus on the lsaA gene. *Microorganisms* https://doi.org/10.3390/microorganisms9030491 (2021).
51. Seemann, T. Prokka: rapid prokaryotic genome annotation. *Bioinformatics* **30**, 2068–2069 (2014).
52. Page, A. J. et al. Roary: rapid large-scale prokaryote pan genome analysis. *Bioinformatics* **31**, 3691–3693 (2015).
53. Fan, F. et al. The outer-membrane protein TolC of Vibrio cholerae serves as a second cell-surface receptor for the VP3 phage. *J. Biol. Chem.* **293**, 4000–4013 (2018).
54. Metcalf, W. W. et al. Conditionally replicative and conjugative plasmids carrying lacZ alpha for cloning, mutagenesis, and allele replacement in bacteria. *Plasmid* **35**, 1–13 (1996).
55. Gama, J. A., Zilhão, R. & Dionisio, F. Conjugation efficiency depends on intra and intercellular interactions between distinct plasmids: Plasmids promote the immigration of other plasmids but repress co-colonizing plasmids. *Plasmid* **93**, 6–16 (2017).
56. Neil, K., Allard, N., Grenier, F., Burrus, V. & Rodrigue, S. Highly efficient gene transfer in the mouse gut microbiota is enabled by the Incl(2) conjugative plasmid TP114. *Commun. Biol.* **3**, 523 (2020).
57. Almagro Armenteros, J. J. et al. SignalP 5.0 improves signal peptide predictions using deep neural networks. *Nat. Biotechnol.* **37**, 420–423 (2019).
58. Mirdita, M. et al. ColabFold: making protein folding accessible to all. *Nat Methods* **19**, 679–682 (2022).

59. Ashkenazy, H. et al. ConSurf 2016: an improved methodology to estimate and visualize evolutionary conservation in macromolecules. *Nucleic Acids Res.* **44**, W344–350 (2016).

Acknowledgements
We thank W.L., M.Y., and B.P. of the Department of Diarrheal Diseases for advice on this study and acknowledge the support from the National Key Research and Development Program of China (2022YFC2303900, 2024YFC3406305).

Author contributions
X.L. and B.K. conceived the project and designed the experiments. Z.L. (Zhe Li), X.L., Z.L. (Zhenpeng Li), and Y.P. collected and sorted complete genomes of pMCRs. Z.L. (Zhenpeng Li) helped genome clustering constructions and pan/core-genome analyses. Z.L. (Zhe Li), Y.P., M.Z., and Y.W. performed T4SS gene cluster structure analysis, conjugation experiments, and 3D structure predictions of proteins. Z.L. (Zhe Li) performed the visualization of results and wrote the manuscript with contributions from X.L. and B.K. All authors read and commented on successive drafts, and all approved the content of the final version.

Competing interests
The authors declare no competing interests.

Additional information
Supplementary information The online version contains supplementary material available at https://doi.org/10.1038/s42003-025-07748-y.

Correspondence and requests for materials should be addressed to Xin Lu or Biao Kan.

Peer review information *Communications Biology* thanks CV Srikanth and the other, anonymous, reviewer(s) for their contribution to the peer review of this work. Primary Handling Editors: Ranjana Pathania, Tobias Goris, and David Favero. A peer review file is available.